Front tracking for quantifying advection-reaction-diffusion

Thomas D. Nevins[1,a)] and Douglas H. Kelley[2,b)]
[1]Department of Physics and Astronomy, University of Rochester, Rochester, New York 14627, USA
[2]Department of Mechanical Engineering, University of Rochester, Rochester, New York 14627, USA

(Received 3 February 2017; accepted 22 March 2017; published online 6 April 2017)

We present an algorithm for measuring the speed and thickness of reaction fronts, and from those quantities, the diffusivity and the reaction rate of the active chemical species. This front-tracking algorithm provides local measurements suitable for statistics and requires only a sequence of concentration fields. Though our eventual goal is front tracking in advection-reaction-diffusion, here we demonstrate the algorithm in reaction-diffusion. We test the algorithm with validation data in which front speed and thickness are prescribed, as well as simulation results in which diffusivity and reaction rate are prescribed. In all tests, measurements closely match true values. We apply the algorithm to laboratory experiments using the Belousov–Zhabotinsky reaction, producing speed, diffusivity, and reaction rate measurements that are statistically more robust than in prior studies. Finally, we use thickness measurements to quantify the concentration profile of chemical waves in the reaction. *Published by AIP Publishing*. [http://dx.doi.org/10.1063/1.4979668]

The three physical processes, advection (fluid flow), reaction, and molecular diffusion, govern the dynamics of concentrations in many common systems, including pharmaceutical manufacture,[1] wildfires,[2] chemical waves in the heart,[3] and phytoplankton blooms.[4] Because advection is driven by an underlying fluid flow that is often chaotic or turbulent, and because reaction often involves nonlinear chemical kinetics, complicated concentration dynamics are typical in advection-reaction-diffusion systems. To characterize the concentration field and predict its evolution, a simplified representation is essential. One technique used for making a simplified representation is to choose a concentration threshold and identify the *reaction fronts* separating high-concentration reacted regions from low-concentration unreacted regions. By tracking those fronts and measuring their local speed and thickness, our algorithm can provide characterizations of front dynamics that are more robust to noise, situation, and input parameter choices than were previously available. In the future, such characterizations may enable new predictive theories that incorporate greater detail. Local measurements may also allow the investigation of new questions, such as the relations among local front speed, local front thickness, and local advection speed; or the relation between local front thickness and local front curvature.

I. INTRODUCTION

Advection-reaction-diffusion systems give rise to rich and complex dynamics. When a reaction grows in the presence of a flowing fluid, the flow itself is different from one location to another at each instant. As a direct result of spatial complexity of flows, the reaction grows in different directions from one location to another, and can even grow at different rates from place to place.[5] Studies on the interaction between reaction and advection have shown frozen reaction fronts in porous media,[6,7] and reactions growing at different rates in Poiseuille flow based on the front shape of the reaction.[8–10] Significant global effects of fluid flow on enhanced reaction growth in the bulk are also well known.[1,11,12] Still other studies have found pattern formation among advection driven reactions.[13]

The complex dynamics of advection-reaction-diffusion systems can be modeled in terms of the reaction fronts that separate reacted from unreacted regions. The recently-developed theories of burning invariant manifolds (BIMs) and burning Lagrangian Coherent Structures (bLCS)[14–19] identify barriers to the propagation of fronts caused by opposing advection, enabling some prediction of reaction growth. Thus the theories predict where fronts will advance and where they will not. Calculating those barriers requires knowing the speed at which fronts advance when only reaction and diffusion are present. The front tracking algorithm we describe determines that front speed at many locations, providing a statistically robust measurement. Prior studies have measured front speed only along a single line.[20,21] Instead, our algorithm works from time series of concentration fields, which can be gathered from either simulations or experiments.

The algorithm also determines the front thickness at many locations, that is, the distance over which product concentration varies from small (near zero) to large (near saturation). Through well-known solutions to reaction-diffusion equations, front thickness along with front speed can be used to determine the diffusivity and reaction rate of the reacting species in reactions without flow. By determining front speed and thickness at many locations, the algorithm provides statistically robust measurements of those microscopic quantities as well. Prior studies have typically measured diffusivity and reaction rate at just one location.[22,23]

Though we are interested in modeling advection-reaction-diffusion systems, the discussion below centers on the

a)Electronic mail: tnevins@ur.rochester.edu
b)Electronic mail: d.h.kelley@rochester.edu

theory of reaction-diffusion systems, in which advection is absent. Similarly, the validation and simulation data we use to test the algorithm involve no advection, and the experiments described below involve no advection. Our focus on reaction-diffusion is not an oversight. For validating and verifying a new algorithm, we have chosen reaction-diffusion systems because of their relative simplicity. Their physics is better understood, and we have better intuition about what results to expect from the algorithm. Generalizing front tracking from reaction-diffusion to advection-reaction-diffusion requires only that front displacements due to advection be subtracted off before implementing the algorithm described below, then restored later. This is equivalent to processing the advection term of the advection-reaction-diffusion equation, Eq. (1), separately from the reaction-diffusion, which is a good first-order approximation as long as the flow field is known. The approximation also works best for fast reactions, where the fronts are thin. In these locations the advection term in Eq. (1) is zero except at the fronts. However, we leave further discussion of advection for a future publication.

This paper proceeds as follows: In Section II we explain the theory of reaction-diffusion equations, and how diffusion and reaction rate determine front speed and thickness. In Section III we detail our algorithm and its parameters. Section IV shows that the algorithm measures correct front speed and thickness, working from validation data in which those quantities are prescribed. Section IV also shows the algorithm to be robust to noise and insensitive to parameter choices of the user. In Section V, we apply the algorithm to simulation results, showing that the algorithm measures correct diffusivity and reaction rate, working from simulation results in which those quantities are prescribed. Section VI shows the results of applying the algorithm to laboratory experiments with the Belousov–Zhabotinsky (BZ) reaction, in which front speed, front width, diffusivity, and reaction rate are all measured via the front tracking algorithm. Finally, Section VII summarizes our results and considers implications for future work.

II. RELATING THICKNESS AND SPEED TO DIFFUSIVITY AND REACTION RATE

The growth of a reacted region is governed by its initial shape, the material diffusivity, and reaction rates. That is, the physical constants describing microscopic processes (diffusivity and reaction rate) determine the macroscopic behavior (front speed and thickness). Conversely, measuring macroscopic behavior can reveal microscopic quantities, often through simple algebraic relationships. Though this insight has been published,[6,24] to our knowledge it has not been utilized before, because front thickness has not been measured in the sense described below. However, local reaction profile length scales have been measured using maximum gradient methods in combustion,[25,26] and reaction profiles of the BZ reaction have been photographed.[27] In this section we describe the mathematical connections between diffusivity, reaction rate, front speed, and front thickness.

We are interested in systems governed by the advection-reaction-diffusion equation

$$\frac{dc}{dt} = (\boldsymbol{u}\cdot\nabla)c + D\nabla^2 c + F(c), \tag{1}$$

where c is the concentration of the reaction product, $\boldsymbol{u}$ is the underlying flow, D is the product diffusion coefficient, and $F(c)$ specifies the reaction kinetics. We define a front as a line (or in three-dimensional reactions, a surface), which separates reacted and unreacted regions. In particular, a front is a particular level curve or surface of the concentration field c. For fast fronts, the changes from the unreacted to the reacted state occur in a very short spatial distance, so a change in the choice of which level curve is used results in only a small change in curve position. Far from a front, whether it is thin or thick, very little change occurs in c, so the front is the dominant feature of a reaction. The novelty of the algorithm lies not in locating fronts, which can be done by simple thresholding, but in quantifying their velocity and thickness.

If the advection term is zero, Eq. (1) simplifies to the reaction-diffusion equation

$$\frac{dc}{dt} = D\nabla^2 c + F(c). \tag{2}$$

Since diffusion spreads scalars down the gradient of their own concentration fields, it spreads reacted regions *perpendicular* to their concentration level curves. Since the reaction term $F(c)$ is local, it only serves to raise or lower concentration. Therefore, a reaction-diffusion front always moves down the concentration gradient, locally perpendicular to the front itself.

Moreover, because the spatial variation of concentration along a reaction front is zero, the diffusion term $D\nabla^2 c$ is dominated by gradients locally perpendicular to the front, so that Eq. (2) can be written in terms of one spatial coordinate x, locally perpendicular to the front. If the reaction term has second-order dynamics, the result is the Fisher Equation

$$\frac{dc}{dt} = D\frac{\partial^2 c}{\partial x^2} + kc_0 c(1-c), \tag{3}$$

where now c is dimensionless, having been normalized by c_0, an equilibrium concentration. Considering the boundary conditions $c=0$ at $x=x_0$ and $c=1$ at $x=-x_0$, and choosing $x_0\to\infty$, the solution to the Fisher Equation[28,29] is

$$c(x,y,t) = \frac{1}{\left(1+e^{(x-vt)/L}\right)^2}, \tag{4}$$

where the front thickness and velocity are

$$L = \sqrt{\frac{6D}{\alpha}}, \tag{5}$$

$$|v| = \frac{5}{6}\sqrt{6D\alpha}, \tag{6}$$

respectively. Here D is the diffusion coefficient and $\alpha = kc_0$ is the reaction rate normalized by equilibrium concentration. Note that the sign of v causes front to move towards the

unreacted region. Also notice that L is not an arbitrary length scale, but a physical distance which relates to the solution for a second order reaction. Equations (5) and (6) can be solved for D and α

$$D = \frac{|v|L}{5}, \tag{7}$$

$$\alpha = \frac{6|v|}{5L}, \tag{8}$$

where we use the speed, $|v|$, to emphasize that this also works for Eq. (3) under the opposite boundary conditions.

In practice, specifying boundary conditions at infinity is an idealization, but the resulting solution closely approximates the true situation as long as $x_0 \gg L$. Also, though curvature of a front is known to alter its speed,[30] solutions of Eqs. (3) and (1) match as long as the radius of curvature of the front is much larger than the length scale used for calculating spatial gradients.

Equations (7) and (8) make it possible to determine the microscopic physical constants D and α by measuring the macroscopic properties L and v—if the chemical kinetics are second order. Similarly, for third order kinetics

$$\frac{dc}{dt} = D\nabla^2 c + kc_0^2 c^2(1-c), \tag{9}$$

which is solved by[6,24]

$$c(x,y,t) = \frac{1}{(1+e^{-(x-vt)/L})}, \tag{10}$$

where the front thickness and speed are

$$L = \sqrt{\frac{2D}{\alpha}}, \tag{11}$$

$$|v| = \sqrt{\frac{D\alpha}{2}}, \tag{12}$$

respectively. Again it is straightforward to write D and α in terms of L and v

$$D = L|v|, \tag{13}$$

$$\alpha = \frac{2|v|}{L}. \tag{14}$$

In fact, the diffusivity and reaction rate can be written in terms of front thickness and speed for chemical kinetics of any order for which the appropriate one-dimensional reaction-diffusion equation can be solved analytically. In this paper we consider experiments and simulations where the reactants are dissolved in water and the reaction is second-order. Therefore L and $|v|$ are henceforth defined as in Eqs. (5) and (6). We suspect the method works even better for third-order reactions, because the form of the solution for third-order dynamics makes fits to measurements more straightforward. We have not attempted the method on any other reaction types, but we see no reason that it would not work on different chemistries, such as combustion, or even solid- or gas-phase reactions.

III. FRONT TRACKING

In this section we describe the algorithm to locally measure front thickness and speed in reaction-diffusion systems using a series of concentration fields measured at regular intervals and on a regular spatial grid. The algorithm can be immediately generalized to advection-reaction-diffusion systems as long as the velocity field $\boldsymbol{u}$ is known, either because the system is simulated, or by measuring the flow using particle image velocimetry or particle tracking velocimetry. Written in MATLAB, the open-source algorithm is freely available.[31] An example of the end result is shown in Figure 1.

The algorithm begins by locating reaction fronts, which are defined as the surfaces that separate regions of high product concentration $c > c_{\text{thresh}}$ from low product concentration $c < c_{\text{thresh}}$, where c_{thresh} is a user-defined concentration threshold. (Throughout this paper, we consider the simplified case of reaction in a thin layer that can be approximated as two-dimensional, in which reaction fronts are one-dimensional curves, not two-dimensional surfaces. However, the algorithm should readily generalize to three-dimensional systems.) After finding the edges of regions where $c > c_{\text{thresh}}$, the algorithm smooths those edges because measuring concentration on a discrete grid makes the edges rough at grid scale and does not accurately represent the front shape. This smoothing is done using a sliding line fit spanning S points along the boundary. In this process S neighbors are fit to a line which is then used to adjust the central point's location. Line smoothing is always necessary for accurate reconstruction of perpendiculars, since

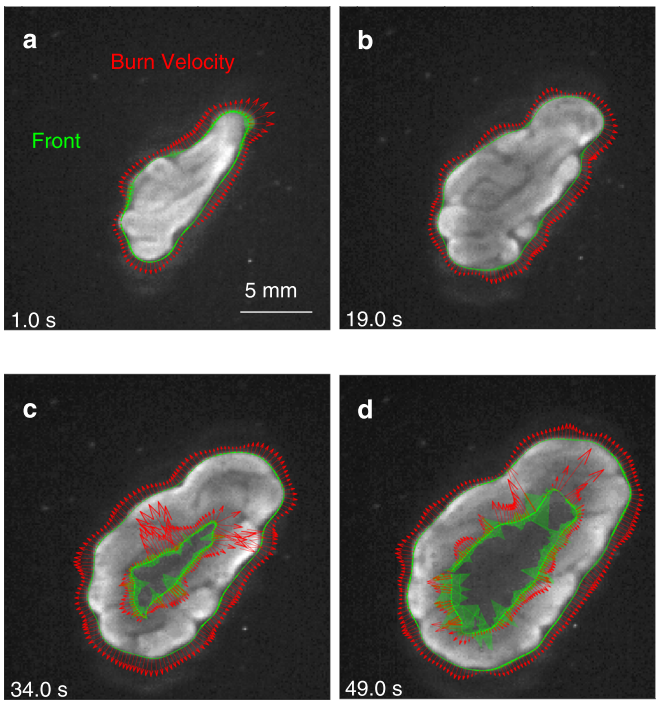

FIG. 1. Example results of front tracking. Grayscale images are snapshots of a reaction-diffusion experiment with the Belousov–Zhabotinsky (BZ) reaction, described below. Front location is indicated in green, with the green area indicating local front thickness; local front velocity is indicated by red arrows.

TABLE I. Parameters chosen by the algorithm's user.

Parameter	Description
c_{thresh}	Concentration threshold
S	Span of sliding fit for smoothing fronts
A_{min}	Minimum area of reacted regions
M	Size of excluded margin
d_{max}	Maximum front displacement
n_{skip}	Number of concentration fields skipped when measuring speeds
L_{fit}	Half profile fit length for determining front thickness

boundaries from a thresholded image always follow pixel boundaries. To further reduce noise effects and in anticipation of the addition of small tracer particles to allow velocity measurements in future advection-reaction-diffusion experiments, the algorithm removes high concentration regions whose area is smaller than A_{min}, another user-defined parameter. Finally the algorithm imposes margins by assigning "not-a-number" as the speed and thickness of all front elements within a distance M of the edges of the field of view. This prevents those edges from being incorrectly identified as boundaries. All algorithm parameters, including c_{thresh}, S, A_{min}, and M, are listed in Table I.

Once we have located fronts, we can measure their speed, and Fig. 2 illustrates our algorithm for doing so. First, the algorithm considers the fronts in two subsequent concentration fields. Then, it draws a perpendicular line extending a distance d_{max} in each direction from each point on the earlier front; d_{max} is specified by the user. The algorithm then finds the locations where the perpendicular intersects fronts in the subsequent frame. The displacement between the original point and each intersection is calculated, and the smallest displacement is divided by the delay time between concentration fields, yielding the front speed at that one point. Higher order time steps are certainly possible, but we will show later that this method works well for reaction-diffusion. If the perpendicular intersects no front, a "not-a-number" value is recorded. The process is repeated for every other point on the fronts in the earlier concentration field. To eliminate noise caused by high-frequency changes in the concentration field, the algorithm can implement a simple low-pass temporal filter by skipping n_{skip} subsequent concentration fields, as specified by the user. Assuming the grid spacing and interval between concentration fields are known, front speed can be expressed in physical units.

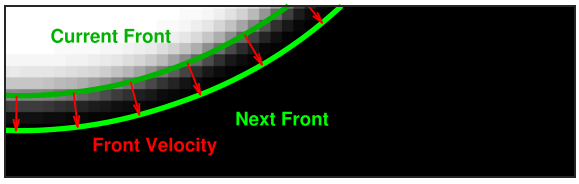

FIG. 2. Algorithm for measuring front velocity. First, the edges of regions where the local concentration c exceeds the chosen threshold c_{thresh} are, after smoothing, identified as fronts. The process is repeated for a subsequent concentration field. The distance between the first and subsequent location of a front perpendicular to the first, along with the delay time between concentration fields, provides the local velocity.

Once we have located fronts, we can also measure their thickness, and Fig. 3 depicts our algorithm for doing so. Only one concentration field need be considered. The algorithm again draws a perpendicular at each point along each front, as in velocity measurement, but with length L_{fit}, specified by the user. The algorithm interpolates the concentration on the regular grid to a set of points along the perpendicular to obtain a concentration profile as shown. That profile is fit to the corresponding one-dimensional solution to the reaction diffusion equation, Eq. (4), yielding the local thickness L. In the process of fitting we need to determine which side of a front is reacted, in order to use a profile shape matching the boundary conditions. This can easily be done by comparing the mean concentration on each half of the profile. This has the added bonus of identifying if the front is fading or growing. Curve fitting allows the use of many data points to measure one number, so L may be a fraction of a pixel length. This is analogous to fitting tracer particles to get sub-pixel accuracy in particle tracking.[32] Assuming the grid spacing is known, front thickness can be expressed in physical units. To ensure accurate fitting L_{fit} should be small enough not to overlap with a nearby front, and no smaller. To see the dependence on L_{fit} and other parameters see Fig. 6.

IV. TRACKING FRONTS IN VALIDATION DATA

To test our algorithm, we first verified that it could reproduce front speed and thickness, given validation data in which speed and thickness had been specified. We created a series of concentration fields in which we constructed fronts of varying shapes, speed, and thickness. Each front had a reaction profile specified by Eq. (4), with $0 \leq c \leq 255$. All validation data are measured in units of pixels and frames. Figure 4 compares the true speeds and thicknesses to the speeds and thicknesses measured using the algorithm. The match is close. The greatest errors in speed occur for a square front and are due to curve smoothing at the sharp corners. These corners move faster than the "true speed". In any physical front, however, diffusion eliminates sharp corners. Measured thicknesses are accurate over a wide range of possible thicknesses. Certain extreme cases can disrupt this accuracy. In particular, as the thickness approaches the size

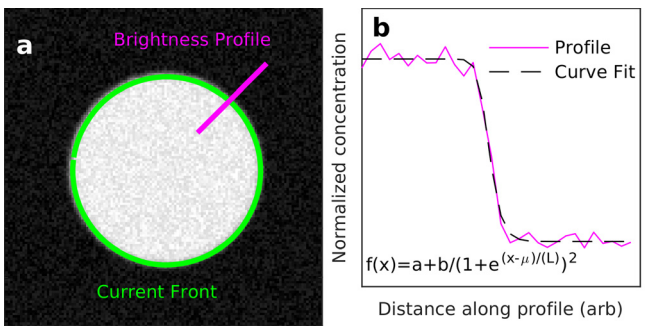

FIG. 3. Algorithm for measuring front thickness, shown using validation data. First, the edges of regions where the local concentration c exceeds the chosen threshold c_{thresh} are, after smoothing, identified as fronts. Then the concentration profile along a line perpendicular to the front is fit to Eq. (4), yielding the local thickness L.

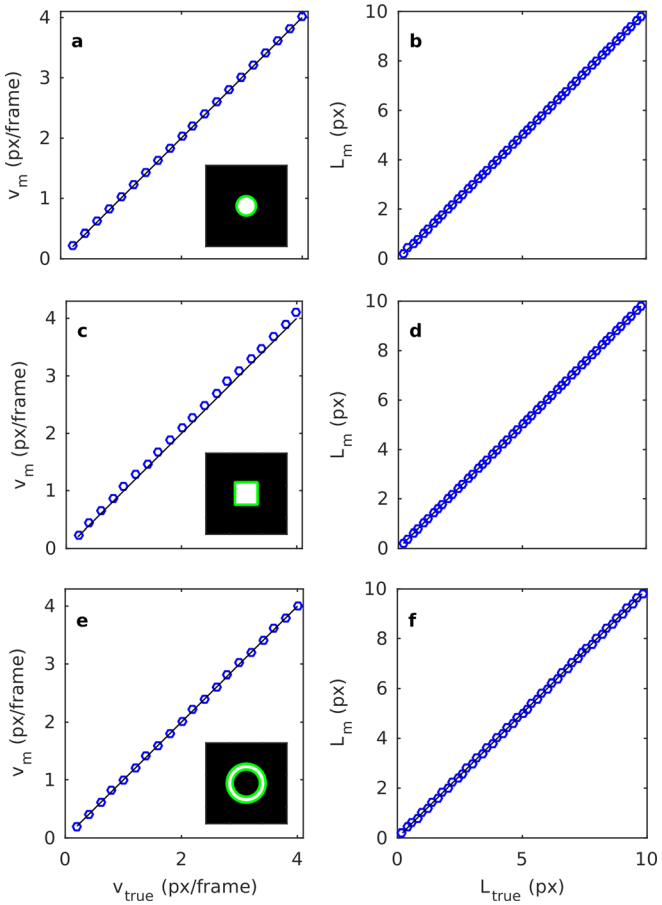

FIG. 4. Measurements of front speed and thickness in validation data, compared with true values, for three different front shapes. (a) Measured median speed v_m of a circular front propagating outward, compared with its true speed v_{true}. (b) Measured median thickness, L_m, of the same circular front, compared with its true thickness L_{true}. Analogous comparisons are shown in (c)–(f) for square and annular fronts, all propagating outward. In each plot, a 45° line would indicate exact agreement. We chose $L_{\text{fit}} = 20$ pixels for all geometries. Measurements agree closely with truth in all cases, indicating a reliable measurement.

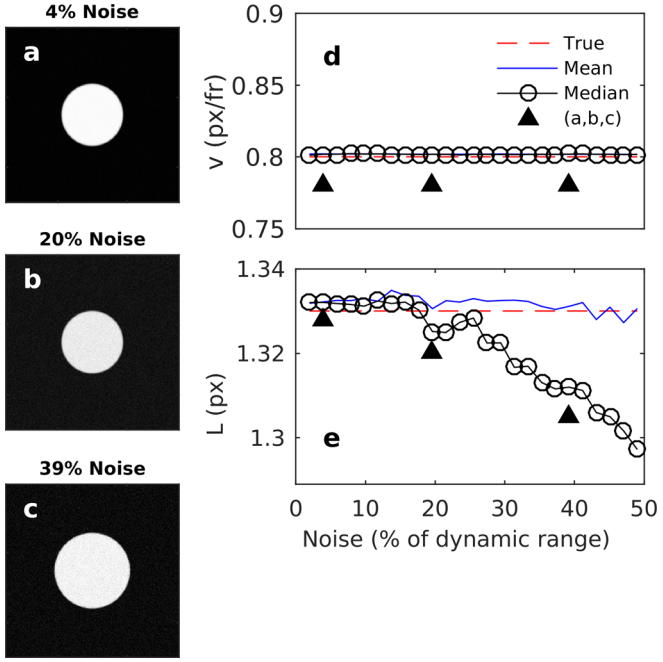

FIG. 5. Robustness of front tracking to noise. (a)–(c) Example concentration fields (validation data) with varying noise magnitude. (d) Noise changes front speed measurements negligibly. (e) Noise with magnitude up to half the dynamic range changes front thickness measurements by about 3%. Arrowheads indicate noise magnitudes corresponding to (a)–(c). Measurements were made using the same default values as in Fig. 6.

of L_{fit}, errors increase. To improve these errors L_{fit} can be increased; here we chose a large fit, $L_{\text{fit}} = 20$ pixels, to reduce the errors. For annuli, as the fronts get thicker, the concentration profiles of the inner and outer boundaries overlap, so that $x_0 \to \infty$ is no longer a good approximation (see Section II). In this case accuracy can be improved by decreasing L_{fit}. Increased resolution reduces error in both speed and thickness.

Next we quantified the robustness of the algorithm to noise in concentration fields. Starting with a circular front as shown in Fig. 4(a), we added uniformly-distributed noise of varying magnitude, and then used our algorithm to measure front speed and thickness. True values were chosen based on preliminary experimental values. Figure 5 shows the results. Speed measurements are essentially unaffected by noise, and errors in thickness measurements grow to just ∼3% when the noise is almost 50% of the dynamic range. One reason these results are robust to uncorrelated noise is that the average speed and thickness are calculated from many local measurements along the entire length of the front; local measurements provide a major advantage. Curve smoothing also helps to remove sudden, incorrect protrusions caused by noise. However, we suspect that the lower-than-expected thickness is due to curve smoothing.

Next we quantified the sensitivity of errors to user choices of the input parameters. Figure 6 shows how front speed and thickness vary with threshold c_{thresh}, profile fit length L_{fit}, and smoothing span S. Errors in speed were typically less than 1%. The only significant error occurs for extremely large smoothing span. Errors in thickness were less than 1% except for $L_{\text{fit}} < 7L$, in which case it seems that there were too few point measurements for a good fit. The algorithm achieves high accuracy despite the fact that all data sets have a noise signal with a peak-to-peak amplitude of 8% of the dynamic range. For very small smoothing span there is no error in thickness, consistent with our expectations that smoothing slightly biases thickness measurements. The algorithm has little sensitivity to the concentration threshold, staying accurate to about 1% for thresholds ranging from 10% to 90% of the maximum concentration.

We found that $d_{\max}$, the maximum front displacement, matters only that it has to be long enough to intersect the next frame's front. Once it is long enough to cross, the accuracy is no longer affected by $d_{\max}$. Likewise, we found insignificant error sensitivity to user choices of $A_{\min}$ and n_{skip}.

V. TRACKING FRONTS IN SIMULATION DATA

Having found the algorithm successful in reproducing front speed and thickness from verification data, we set out to verify that the algorithm could reproduce reaction rate and diffusivity from the results of reaction-diffusion simulations.

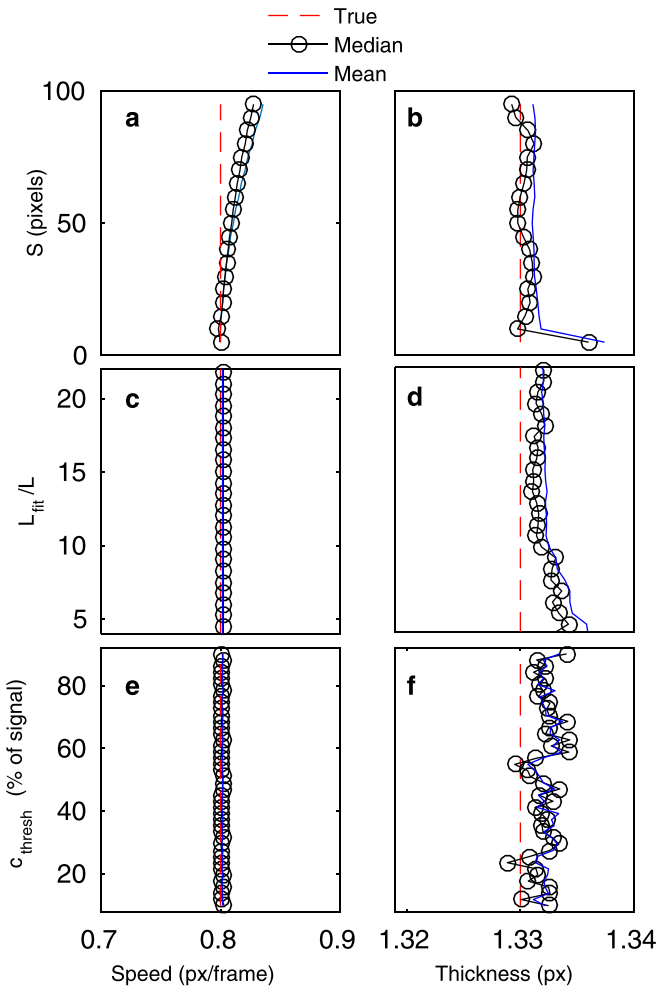

FIG. 6. Sensitivity of front tracking in validation data to input parameters. (a) Variation of front speed with smoothing span S. (b) Variation of front thickness with smoothing span S. Analogous variations are shown for profile fit length L_{fit} (c) and (d) and concentration threshold c_{thresh} (e) and (f). Default parameter values were $c_{\text{thresh}} = 50\%$, $L_{\text{fit}} = 20$ pixels, $S = 20$ pixels, $n_{\text{skip}} = 5$ frames, and $d_{max} = 20$ pixels. In each sequence of measurements, only one parameter was changed, and 8% noise was included.

We wrote a simple two-dimensional simulation that calculates concentration c as it evolves through time according to Eq. (3), using central differences for spatial gradients, first-order time integration, and periodic boundary conditions. We simulated concentration in a two-dimensional domain $-3\pi \le x < 3\pi, -\pi \le y < \pi$, where x and y are now Cartesian coordinates measured in mm and discretized on a 2400×30 rectangular grid (7.85 μm grid spacing in the x-direction). The initial condition was a straight front of the form

$$c(x, y, 0) = \frac{1}{\left(1 + e^{-(x-\mu)/L}\right)^2}, \tag{15}$$

invariant in y, with D and α specified. The y direction was only included to make the final result a field which could be processed cleanly by our algorithm, which is written for two-dimensional concentration fields. Invariance in y also eliminates curvature effects. To ensure convergence, the time step was 9.25×10^{-6} s. Each simulation was run for 4 800 000 time steps, giving 44.4 s of effective data. That duration provided ample data but prevented the front from wrapping around the periodic domain. We then applied our front tracking algorithm to the concentration fields produced by the simulation, obtaining speeds and thicknesses. For each simulation, we recorded the average speed and thickness, and then used them to calculate D and α according to Eqs. (7) and (8).

Figure 7 compares true reaction rates and diffusivities to the values measured using the algorithm. Only one combination D and α gives greater than 5% error, and it is for a case with a low D. Errors in diffusivity are larger than in reaction rate, and diffusivity is consistently over-estimated by the algorithm. We attribute this systematic error not to a problem with the tracking algorithm but to the presence of numerical diffusion in the simulation, caused by estimating continuous derivatives as discrete differences. In fact, when we increased the number of grid points to make numerical gradients more accurate, the error in diffusivity dropped. Larger reaction rate also tends to exacerbate errors produced by numerical diffusion. Errors in reaction rate are very small, and may also be due to numeric diffusion.

VI. TRACKING FRONTS IN EXPERIMENTAL DATA

Having found the algorithm successful with both validation data and simulation results, we applied it to laboratory experiments using the Belousov–Zhabotinsky (BZ) reaction.[24,29,33–35] BZ is a complicated oscillating chemical reaction, often parametrized with the Oregonator model.[36] BZ oscillates between states by passing electrons back and forth with a catalyst. In our case the catalyst is ferroin indicator, so the BZ oscillates between blue and red. The reactions that turn BZ blue are well-modeled as second-order because

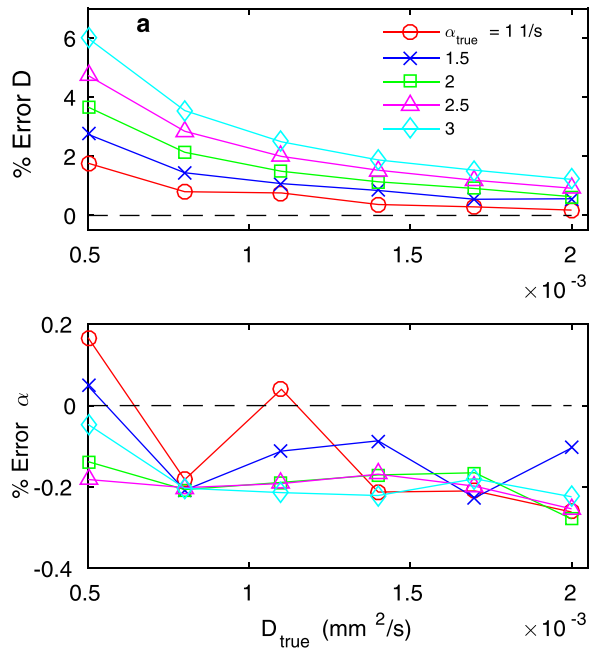

FIG. 7. Accuracy of diffusivity and reaction rate measurements made by tracking fronts in simulation results. The true diffusivity, D_{true}, is given by the position along the horizontal, and the true reaction rate, α_{true}, by the legend. Errors are small and primarily due to numerical diffusion in the simulation, not errors in front tracking.

higher-order reaction terms are negligible.[24] However, the reactions that turn BZ back from blue to red are not well-modeled as second-order. Thus we would expect "fronts" and "backs" to show measurably different behavior when tracked. Recent studies of BZ in gels have also shown interesting phenomena such as autochemotaxis.[37]

We prepared a 2-mm deep layer of BZ solution using the same chemical concentrations as Gowen and Solomon,[19] and then immersed a silver wire for ∼20 s to initiate reaction. We measured the temperature to be 20 °C with a thermocouple, and found the temperature to be constant over the course of each experiment. We illuminated experiments with blue light-emitting diodes and filmed BZ using a grayscale, high-speed camera (Emergent HS-4000M) behind a blue band-pass filter. The higher the concentration of blue ferroin, the more light is passed through the BZ and reflected by a white background. The filter blocks light from unreacted regions so that reacted regions appear bright and unreacted regions appear dark. The transmittance is related to concentration,[33] so the brightness measured by the camera provides an idea of the local concentration of the reacted state. We recorded image sequences for 1–5 min, until spurious fronts from the boundaries of our vessel invaded the field of view. The value of n_{skip} is set so that we take measurements every 1 s; frame rates were usually 3–5 Hz. The spatial resolution was 0.1218 mm/pixel for experiments with circular fronts, and 0.0726 mm/pixel for experiments with planar fronts. We applied our front-tracking algorithm to image sequences produced from experiments, measuring front speed, front thickness, diffusivity, and reaction rate.

Figure 8 shows the distributions of speed and thickness obtained from an experiment with a clear front and back, both growing out from a point trigger. The front and back have nearly the same mean speed, though the back has a broader speed distribution. Measuring identical speeds for fronts and backs is consistent with our physical expectations.

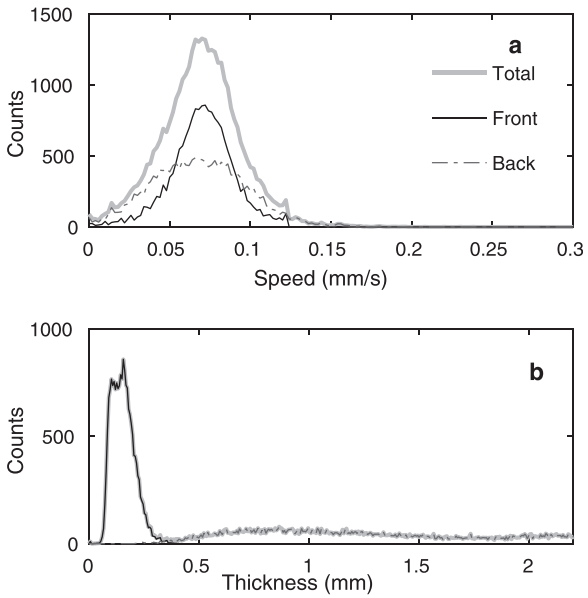

FIG. 8. Histograms of front speeds (a) and thicknesses (b) gathered from an outward-propagating front. Backs have a much wider distribution of thicknesses.

Because BZ oscillates with a fixed duration, each back must have a speed matching the front that came before it. However, the front and the back differ starkly in their thickness. Nearly every measurement of front thickness is close to 168 μm, whereas measurements of back thickness vary from 0.5 mm to 2.5 mm. As expected, the different chemical kinetics of fronts and backs yield different macroscopic behavior.

Considering just the front, which is well-modeled by second-order kinetics, we can extract well-defined values of v and L from histograms like those shown in Fig. 8, and then calculate D and α from v and L. Because BZ is actually a complex chain reaction, the values we measure correspond to rate-limiting steps. We use the modal value of v and L (at the peak of each distribution) because the distributions are not symmetric; their large skews cause mean and median to be poor indicators of typical front dynamics.

In practice, ferroin concentration is often varied during laboratory experiments with BZ, because its colors fade slowly over time, and adding more ferroin restores their contrast. Prior studies found that BZ front speed varies little with ferroin concentration,[33,38] but to our knowledge thickness, diffusivity, and reaction rate have not been considered. We performed two sets of experiments with varying ferroin concentrations, one with circular fronts and one with planar fronts, then extracted v and L, and calculated D and α. For all sets, at least 1500 data points are taken; however, for circular most data sets contain over 8000 points, and for planar all data sets have at least 20 000 points, and most have over 70 000. The results are shown in Fig. 9. In both cases and especially with linear fronts, we see essentially no variation of v with ferroin concentration. In six of the seven experiments, 71 μm/s $\leq v \leq$ 73 μm/s. For comparison, prior studies found $v = 95\,\mu$m/s at 25 °C,[38] 65 μm/s at 18 °C,[33] and 70 μm/s at 20 °C,[14] all using slightly different recipes for BZ. Our recipe matches Bargteil and Solomon[14] and is similar to

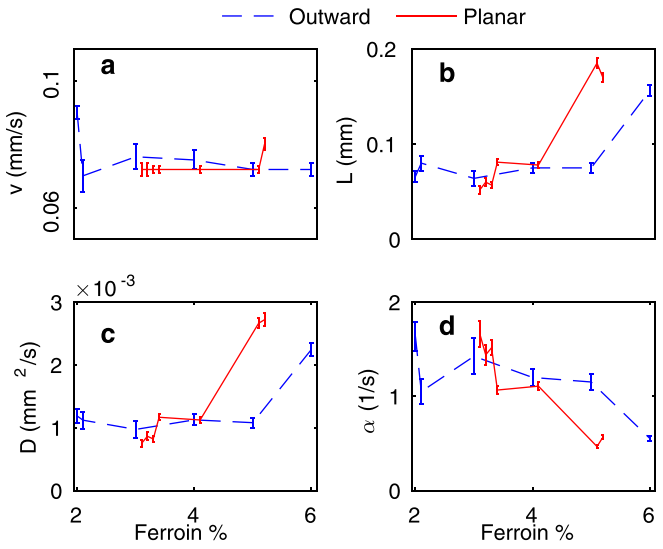

FIG. 9. Effects of ferroin concentration on (a) front speed, (b) front thickness, (c) diffusivity, and (d) reaction rate. In (a) and (b), error bars indicate the bin size of the histograms whose peaks are the measurements; other error sources are smaller. In (c) and (d), indicated errors are propagated from the errors in (a) and (b). In all cases, ferroin concentrations were integer percentages, but plot symbols have been offset slightly for readability.

Field and Noyes.[38] Probably the variation in measured speeds is due more to variations in temperature than to variations in recipe. And though front speed is known to depend on curvature,[30] we measure no obvious variation with curvature in these experiments. However, we measure the mode of the speed and thickness, which is insensitive to large curvature areas which occupy little of any dataset. We measure front speeds consistent with prior results.

To our knowledge, neither front thickness nor back thickness has been measured before in BZ (though profiles have been imaged before[27]). We find that front thickness increases with ferroin concentration, as shown in Fig. 9. However, since ferroin concentration can be increased between experiments, but never decreased except by mixing a new batch of BZ solution, ferroin concentration necessarily correlates with the age of the batch. When the data points shown in Fig. 9 are arranged in chronological order instead, the trend is maintained even if several data points were taken with the same ferroin concentration. We found thickness to depend on ferroin concentration (or age) for both planar and circular fronts. In both cases thickness is steadily around 70 μm, until the BZ has aged or gotten enough ferroin. At this point its thickness jumps to around 170 μm. Further work would be needed to understand what causes the jump from the "low-thickness" data to the "high-thickness" data.

We measure diffusivity and reaction rate to be of the same order of magnitude found in prior studies, which measured $D = 2 \times 10^{-3}\,\mathrm{mm^2/s}$,[24] $D = 1.8 \times 10^{-3}\,\mathrm{mm^2/s}$,[38] and $D = 1.3 \times 10^{-3}\,\mathrm{mm^2/s}$.[39] The average "low-thickness" diffusivity we measured is $D = 1.0 \times 10^{-3}\,\mathrm{mm^2/s}$, matching that of Kuhnert *et al.*[39] most closely. For the "high-thickness" datasets this average is $D = 2.5 \times 10^{-3}\,\mathrm{mm^2/s}$. For BZ, $\alpha = k[\mathrm{BrO_3^-}][\mathrm{H^+}]$. Using our measurements of α and taking $[\mathrm{BrO_3^-}] = 0.06M$ and $[\mathrm{H^+}] = 0.8$ from the literature,[24] we estimate the reaction rate constant in our experiments to be $k = 27\,\mathrm{M^{-2}/s}$ for low thickness, and $k = 11\,\mathrm{M^{-2}/s}$ for large thickness. The first value resolves a contradiction in the literature. Field and Noyes[38] developed a theoretical relationship for front speed which involves the coefficient $(4Dk)^{1/2}$. The authors measured it to be $24.75\,\mathrm{M^{-1}mm\ min^{-1}}$, but predicted $509\,\mathrm{M^{-1}mm\ min^{-1}}$ based on available values of D and k. We repeat the calculation using our measurements and arrive at the value $22\,\mathrm{M^{-1}mm\ min^{-1}}$, closely matching their experimental value and showing that their estimates of D and k may have been mistaken. The "high-thickness" results come out to a value of $20\,\mathrm{M^{-1}mm\ min^{-1}}$. Further confirmation for our reaction rate comes from a measurement by Kuhnert *et al.*,[39] who found $k = 30 \pm 4\ \mathrm{M^{-2}s}$ at 30 °C.

Beyond measuring coefficients, local front tracking also allows us to quantitatively compare the concentration profiles of BZ fronts and BZ backs. While backs are not second-order fronts, the shape of the solution for second order roughly approximates their shape. Distributions of our thickness measurements, like the one shown in Fig. 8, always show two peaks, exactly corresponding to fronts and backs. At any given time, the thickness is the only parameter for a reaction profile. Figure 10 shows profile curves of BZ fronts and backs, using the form given by Eq. (4), with thicknesses

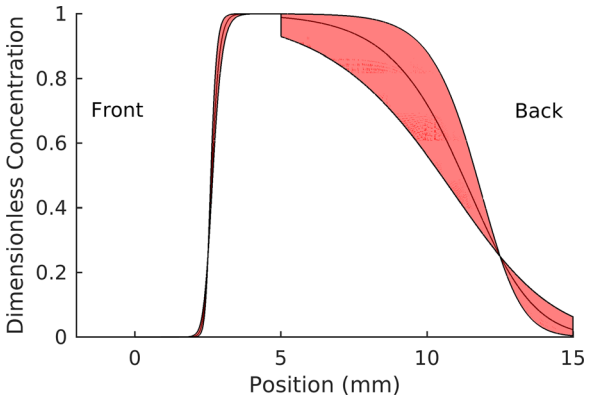

FIG. 10. Measured concentration profile of chemical waves in the BZ reaction. The curve shows the most likely profile, and the shaded region represents the interquartile (middle 50%) of possible profiles. Front and back are shown farther apart than their actual separation, which depends on the reaction's oscillation time and is not indicated here.

corresponding to the most likely values for fronts and backs, taken from Fig. 8. Considering the middle 50% of thickness values for either of the peaks, we can predict that the true profile shape (with fixed μ) has a 50% chance of lying in the range, which is shaded in Fig. 10. The range is much wider for backs, probably because second-order reaction kinetics are a poorer approximation than for fronts. Regardless, whereas similar curves were hypothesized and qualitatively sketched in prior publications,[24] with local front tracking we have been able to provide a quantitative, statistical characterization of the concentration profile of chemical waves in BZ. To our knowledge, ours is the first such quantitative characterization.

VII. SUMMARY AND FUTURE WORK

We have presented a new algorithm for tracking the fronts that separate reacted regions from unreacted regions in advection-reaction-diffusion systems, and for measuring the speed and thickness of those fronts. By repeating the process at many points along fronts, the algorithm can measure spatial variations in front speed and thickness, as well as provide large numbers of measurements appropriate for statistical analysis. Further, we have shown that the algorithm also produces measurements of diffusivity and reaction rate. We demonstrated that the algorithm made accurate measurements when applied to validation data and simulation results. In both cases, results varied less than 1% over a wide range of the user-defined parameters the algorithm requires. Finally we applied the algorithm to laboratory experiments with BZ and obtained statistics of front speed with a mean similar to published values.

This new algorithm offers practical advantages over existing methods. Reaction rate and diffusion are regularly measured with *in situ* chemical tests, but specialized equipment like spectroscopes and magnetic resonance imaging machines are typically required. Our method measures diffusivity and reaction rate with just a camera, making it less expensive and less invasive. However, it is also compatible with concentration fields produced with more complicated instruments and simulations. Our method is independent of

length scale and timescale; it requires only that camera speed and magnification be sufficient to capture the front dynamics.

Finally, the algorithm we present enables future investigations that were not possible before. We have measured the front speed and thickness in one chemical system, the BZ reaction; speed and thickness can immediately be measured in many other chemical systems as well. Diffusivity and reaction rate may also be measureable in other chemical systems, as can the concentration profiles of fronts in those reactions (as in Fig. 10). Because the algorithm is local in that it determines the speed and thickness at many locations along many fronts, it opens the door to studies of spatial variation. For example, front speed has long been known to depend on front curvature,[30] but how does front thickness depend on curvature? Having built confidence that the algorithm accurately tracks fronts in reaction-diffusion systems, we intend to apply it to advection-reaction-diffusion by simultaneously measuring the flow field and accounting for its effect on fronts. Going further, local measurements of front speed and velocity might allow simplified models of advection-reaction-diffusion in terms of the fronts themselves. Finally, the algorithm can be generalized in a straightforward way to work with three-dimensional concentration fields.

ACKNOWLEDGMENTS

The authors are grateful for insightful conversations with N. T. Ouellette and J. G. Puckett.

[1]C. P. Schlick, P. B. Umbanhowar, J. M. Ottino, and R. M. Lueptow, Chaos **24**, 013109 (2014).
[2]C. Punckt, P. S. Bodega, P. Kaira, and H. H. Rotermund, J. Chem. Educ. **92**, 1330 (2015).
[3]A. T. Winfree, J. Biosci. **27**, 465 (2002).
[4]A. P. Martin, Prog. Oceanogr. **57**, 125 (2003).
[5]T. D. Nevins and D. H. Kelley, Phys. Rev. Lett. **117**, 164502 (2016).
[6]S. Saha, S. Atis, D. Salin, and L. Talon, Europhys. Lett. **101**, 38003 (2013).
[7]S. Atis, S. Saha, H. Auradou, D. Salin, and L. Talon, Phys. Rev. Lett. **110**, 148301 (2013).
[8]B. F. Edwards, Phys. Rev. Lett. **89**, 104501 (2002).
[9]B. F. Edwards, Chaos **16**, 043106 (2006).
[10]M. Leconte, J. Martin, N. Rakotomalala, and D. Salin, Phys. Rev. Lett. **90**, 128302 (2003).
[11]Z. Neufeld, Phys. Rev. Lett. **87**, 108301 (2001).
[12]P. E. Arratia and J. P. Gollub, Phys. Rev. Lett. **96**, 024501 (2006).
[13]V. Pérez-Muñuzuri and G. Fernández-García, Phys. Rev. E **75**, 046209 (2007).
[14]D. Bargteil and T. Solomon, Chaos **22**, 037103 (2012).
[15]J. Mahoney, D. Bargteil, M. Kingsbury, K. Mitchell, and T. Solomon, Europhys. Lett. **98**, 44005 (2012).
[16]K. A. Mitchell and J. R. Mahoney, Chaos **22**, 037104 (2012).
[17]J. R. Mahoney and K. A. Mitchell, Chaos **23**, 043106 (2013).
[18]J. R. Mahoney and K. A. Mitchell, Chaos **25**, 087404 (2015).
[19]S. Gowen and T. Solomon, Chaos **25**, 087403 (2015).
[20]J. A. Pojman, R. Craven, and D. C. Leard, J. Chem. Educ. **71**, 84 (1994).
[21]K. Kovacs, M. Leda, V. K. Vanag, and I. R. Epstein, Physica D **239**, 757 (2010).
[22]C. Gendrin, Y. Roggo, and C. Collet, J. Pharm. Biomed. Anal. **48**, 533 (2008).
[23]E. Ray, P. Bunton, and J. A. Pojman, Am. J. Phys. **75**, 903 (2007).
[24]S. K. Scott, *Oscillations, Waves, and Chaos Iin Chemical Kinetics* (Oxford University Press Inc., New York, 1994).
[25]A. Buschmann, F. Dinkelacker, T. Schafer, M. Schafer, and J. Wolfrum, *Measurement of the Instantaneous Detailed Flame Structure in Turbulent Premixed Combustion* (TECFLAM, Stuttgart, 1987), pp. 437–445, oCLC: 76442353.
[26]L. P. H. de Goey, T. Plessing, R. T. E. Hermanns, and N. Peters, Proc. Combust. Inst. **30**, 859 (2005).
[27]S. C. Müller, T. Plesser, and B. Hess, Physica D **24**, 87 (1987).
[28]M. J. Ablowitz and A. Zeppetella, Bull. Math. Biol. **41**, 835 (1979).
[29]V. K. Vanag and I. R. Epstein, J. Chem. Phys. **117**, 8508 (2002).
[30]P. Foerster, S. C. Muller, and B. Hess, Science **241**, 685 (1988).
[31]See http://www.me.rochester.edu/projects/dhkelley-lab/FrontTracking.zip to download of the Front Tracking computer code.
[32]N. T. Ouellette, H. Xu, and E. Bodenschatz, Exp. Fluids **40**, 301 (2006).
[33]P. M. Wood and J. Ross, J. Chem. Phys. **82**, 1924 (1985).
[34]I. R. Esptein, Chem. Eng. News **65**, 24 (1987).
[35]A. N. Zaikin and A. M. Zhabotinsky, Nature **225**, 535 (1970).
[36]R. J. Field and R. M. Noyes, J. Chem. Phys. **60**, 1877 (1974).
[37]P. Dayal, O. Kuksenok, and A. C. Balazs, Proc. Natl. Acad. Sci. U. S. A. **110**, 431 (2013).
[38]R. J. Field and R. M. Noyes, J. Am. Chem. Soc. **96**, 2001 (1974).
[39]L. Kuhnert, H. J. Krug, and L. Pohlmann, J. Phys. Chem. **89**, 2022 (1985).